Thermochimica Acta 512 (2011) 142–149

Contents lists available at ScienceDirect

Thermochimica Acta

journal homepage: www.elsevier.com/locate/tca

Thermal stability studies on clay nanocomposites prepared from a degradable poly(ester amide) constituted by glycolic acid and 6-aminohexanoic acid

Laura Morales-Gámez[a,b], Lourdes Franco[a,b], Jordi Puiggalí[a,b,*]

[a] Departament d'Enginyeria Química, Universitat Politècnica de Catalunya, Av. Diagonal 647, E-08028, Barcelona, Spain
[b] Centre de Recerca en NanoEnginyeria (CRNE), Universitat Politècnica de Catalunya, Edifici C', c/Pascual i Vila s/n, E-08028, Barcelona, Spain

ARTICLE INFO

Article history:
Received 20 June 2010
Received in revised form
14 September 2010
Accepted 19 September 2010
Available online 29 September 2010

Keywords:
Nanocomposites
Kinetic analysis
Non-isothermal thermogravimetry
Poly(ester amide)
Thermal degradation

ABSTRACT

An intercalated nanocomposite of the organically modified montmorillonite Cloisite C25A and a degradable poly(ester amide) based on glycolic acid and 6-aminohexanoic acid units (poly(glc-*alt*-amh)) was prepared using a twin-screw co-rotating extruder. The non-isothermal degradation kinetics was investigated by thermogravimetric analysis (TG and DTG) in the temperature range of 50–600 °C at five heating rates (2, 5, 10, 20 and 40 °C/min) and compared with the neat polymer. Significant differences were found since the nanocomposite showed three degradation steps instead of the two decomposition processes detected in the pristine sample. The onset mass loss temperature decreased in the nanocomposite due to the presence of the organo-modifier compound, but the presence of the silicate layers significantly decreased the degradation rate at the last stages of decomposition. Kinetic analysis was performed using the Kissinger method and the isoconversional (Kissinger–Akahira–Sunose and Friedman) methods. The true kinetic triplets (E, A, $f(\alpha)$) were determined for the first two steps of degradation through the Coats–Redfern and the Invariant Kinetic Parameters methods. The results clearly indicated that the presence of the organo-modified clay modified the mechanisms of degradation.

1. Introduction

Development of new biodegradable polymers is a subject of great interest due to their applications as both commodity and speciality materials [1,2]. The increasing demand of such materials and even the strict requirements needed to fulfil determined user specifications have conducted to the study of new families and also to the modification of properties by preparation of nanocomposites.

Poly(ester amide)s are considered a promising family of biodegradable polymers since can combine a degradable character caused by the existence of hydrolizable ester groups (–COO–) with relatively good thermal and mechanical properties afforded by the strong intermolecular hydrogen bond interactions established between their amide groups (–NHCO–) [3–6]. A synthetic route based on the formation of metal halide salts as the driving force of a thermal polycondensation reaction was recently proposed and successfully applied to prepare alternating copolymers of glycolic acid and ω-amino acids [7,8] such as the 6-aminohexanoic acid derivative (hereafter named poly(glc-*alt*-amh)). Different studies have been performed to understand its crystalline structure [9], crystallization behavior [10] and thermal degradation mechanism [11] as well as to demonstrate its biocompatibility [12].

It has also been demonstrated that exfoliated and intercalated nanocomposites based on a poly(glc-*alt*-amh) matrix and the C25A organo-modified clay can be well prepared by the in situ polymerization [13] and the melt intercalation techniques [14], respectively. Incorporation of the layered silicate had a clear influence on properties (e.g., crystallization behaviour) depending on the final structure of the nanocomposite [13,14]. Thus, nucleation was hindered and enhanced in exfoliated and intercalated structures, respectively.

In the present work, we specifically studied the influence of the C25A organo-modified clay on the thermal degradation mechanism of poly(glc-*alt*-amh). We have selected the intercalated nanocomposite prepared by the melt mixing technique, which has the advantage of using a polymer sample with a predefined molecular weight. Thermal degradation has been evaluated under non-isothermal conditions applying different kinetic methods (differential and integral) and the obtained kinetic parameters compared with those previously deduced for the pristine polymer sample [11].

* Corresponding author at: Universitat Politecnica de Catalunya, Departament d'Enginyeria Quimica, Av. Diagonal 647, 08028 Barcelona, Spain.
Tel.: +34 34016684; fax: +34 34017150.
E-mail address: Jordi.Puiggali@upc.es (J. Puiggalí).

0040-6031/$ – see front matter © 2010 Elsevier B.V. All rights reserved.
doi:10.1016/j.tca.2010.09.017

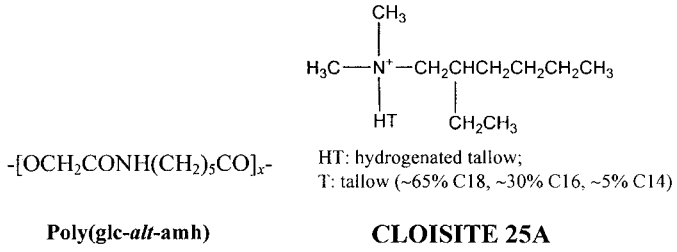

Scheme 1.

2. Experimental

2.1. Materials

Poly(glc-*alt*-amh) was synthesized with an 80% yield by thermal polyesterification of the sodium salt of the N-chloroacetyl-6-aminohexanoic acid [7,8]. The polymer used in this work had an intrinsic viscosity of 0.92 dL/g (dichloroacetic acid at 25 °C), a polydispersity index of 2.10 and a M_n molecular weight of 50,100 g/mol (from GPC analysis).

Dimethyl hydrogenated-tallow 2-ethylhexyl ammonium montmorillonite (CLOISITE 25A, Southern Clay Products, 2MHTEX) was used as received. The chemical structures of the specific surfactant of the organo-modified layered phyllosilicate and the polymer are shown in Scheme 1.

2.2. Preparation of nanocomposite

Nanocomposites containing 3% of C25A clay particles were prepared by melt mixing in two steps using a co-rotating tightly intermeshed twin-screw extruder (DSM Xplore 5 ml microcompounder). All materials were dried under vacuum prior to mixing. The processing temperature, screw rotation and cycle time were 190 °C, 100 rpm and 3 min, respectively.

2.3. Measurements

The structure and distribution of Cloisite were observed with a Philips TECNAI 10 transmission electron microscope (TEM) at an accelerating voltage of 100 kV. TEM specimens were prepared by embedding the film in a low viscosity modified Spurr epoxy resin and curing at 40 °C for a few days and then at 60 °C for 6 h. Ultrathin sections (less than 100 nm) were cut at room temperature using a Sorvall Porter–Blum microtome equipped with a diamond knife. Finally, the sections were collected in a trough filled with water and lifted onto carbon coated copper grids. Interlayer spacing of the clay was studied by wide angle X-ray scattering (WAXD) using a Siemens D-500 diffractometer (Karlsruhe, Germany) with Cu K_α radiation ($\lambda = 0.1542$ nm).

Thermal degradation was determined at heating rates of 2, 5, 10, 20 and 40 °C/min with around 5 mg samples in a Q50 thermogravimetric analyzer of TA Instruments and under a flow of dry nitrogen. The analysis was performed in the temperature range from 50 °C to 600 °C. Deconvolution of the derivative thermogravimetric analysis (DTG) curve was performed with the PeakFit v4 program by Jandel Scientific Software, using an asymmetric function known as "asymmetric double sigmoidal".

3. Results and discussion

3.1. Dispersion structure of the C25A clay in the composite with poly(glc-alt-amh)

Direct observation of the morphology and phase distribution of ultrathin sections of poly(glc-*alt*-amh)/C25A specimens by transmission electron microscopy clearly showed that an intercalated structure was predominant (Fig. 1). In this way, X-ray diffraction profiles of the nanocomposite sample revealed also the existence of a low angle reflection associated to the stacking of silicate layers. The measured spacing was close to 2.68 nm, a higher value than the one observed in the profile of the C25A clay (1.97 nm). Thus, polymer chains in the nanocomposite sample were intercalated in the galleries of the dispersed clay and increased the interlayer spacing.

3.2. Thermal stability of the poly(glc-alt-amh)/C25A nanocomposite

Thermogravimetric scans showed clear differences between the neat polymer and its nanocomposite with the C25A organo-modified clay. In this way, the nanocomposite showed a lower onset degradation temperature for all the assayed heating rates (Table 1), probably due to the lower stability of the organo-modifier compound, and in general a shift of its degradation curve to lower temperatures. However, curves approached to each other at the last stages of degradation suggesting that the neat polymer decomposition at high temperature proceeded faster than in the nanocomposite. Both samples reached a constant weight percentage, the remaining residue was logically greater for the nanocomposite (13% versus to 9%) due its clay content.

The degree of degradation or conversion, α, at a given temperature was calculated as:

$$\alpha = \frac{W_0 - W}{W_0 - W_\infty} \quad (1)$$

where W_0, W and W_∞ were the initial weight, the weight at the considered temperature and the final weight at the end of the degradation process, respectively. Fig. 2 plots the degree of conversion versus temperature (TG curve) of the nanocomposite sample at all the assayed heating rates together with the corresponding derivative curves (DTG). For the sake of completeness, curves of the neat polymer are also shown for a representative heating rate (40 °C/min). The characteristic TG and DTG temperatures for the

Fig. 1. Transmission electron micrograph showing the morphology of the poly(glc-*alt*-amh)/C25A nanocomposite with a Cloisite concentration of 3%. Inset shows the diffraction peak associated to the interlayer spacing observed in the C25A organo-modified clay (dashed line) and the nanocomposite sample (solid line).

Table 1
Thermogravimetric data of the nanocomposite and pristine samples.

Sample	β (°C/min)	T_{onset} (°C)	$T_{0.2}$ (°C)	$T_{0.5}$ (°C)	$T_{0.7}$ (°C)	T_{max} (°C)
Poly(glc-*alt*-amh)[a]	2	207	319	359	411	326/412
	5	220	339	370	423	345/434
	10	232	356	388	433	357/442
	20	240	375	408	451	382/460
	40	260	397	429	471	404/485
Poly(glc-*alt*-amh)/C25A	2	194	321	357	397	316/387/417
	5	215	339	367	409	330/397/437
	10	223	344	386	424	350/428/451
	20	227	357	393	439	363/440/462
	40	249	374	408	452	381/453/481

[a] From Ref. [11].

nanocomposite and the neat polymer sample are summarized in Table 1.

Both samples showed a clear first degradation step which approximately corresponded to a conversion of 0.45–0.50. This step can be mainly associated to the decomposition of the glycolic acid residues as it was previously determined from the study of a series of copolymers derived from different ω-amino acids and consequently with different weight percentages of glycolic acid units [11]. Thermogravimetric traces clearly indicated that this process always ended at lower temperatures for the nanocomposite than for the pristine sample.

DTG curves showed a second degradation step for the neat polymer which was associated to the decomposition of the rich ω-amino acid fraction [11]. This process appeared rather more complicated in the nanocomposite sample since at least two DTG additional peaks were detected at a temperature that increased with the heating rate. Thus, incorporation of clay particles had a remarkable influence on the degradation process which consequently took place according to three differentiated steps. These clear differences between the decomposition of the pristine and the nanocomposite samples demonstrate that the degradation mechanism changed when the organo-modified clay was added and justify undertaking a more detailed kinetic analysis.

Each degradation step of the nanocomposite was then analyzed by mathematical deconvolution of the DTG curves as previously performed with the neat polymer [11]. Fig. 3 shows the separation in three and two peaks of the DTG curves obtained at a representative heating rate of 5 °C/min for the nanocomposite and the pristine polymer, respectively. In all cases, the sum of the separated curves reproduced quite well the experimental signal.

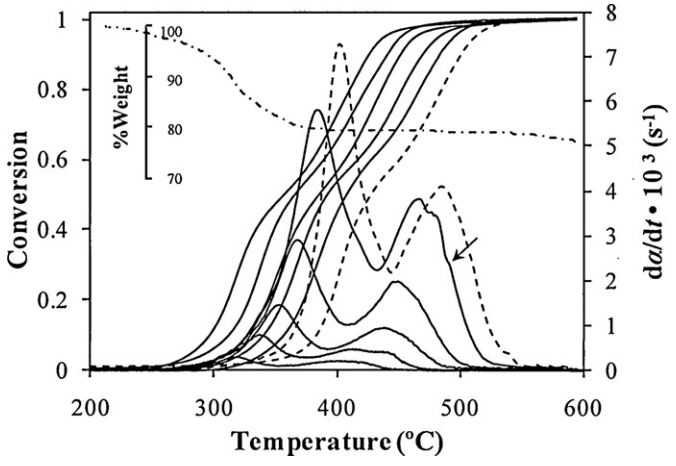

Fig. 2. Degree of conversion (α) versus temperature and derivative curve for the decomposition of poly(glc-*alt*-amh)/C25A nanocomposite at different heating rates. For comparative purpose conversion and derivative curves obtained at 40 °C/min with the neat polymer are also represented (dashed lines). Curves are drawn from left to right in increasing order of heating rates (2, 5, 10, 20 and 40 °C/min). The thermogravimetric curve (-.-.-) of the C25A organomodified clay is also plotted using an extra axis.

3.3. Evaluation of the activation energy for the thermal degradation of the poly(glc-alt-amh)/C25A nanocomposite

According to non-isothermal kinetic theory, thermal degradation of a sample can be expressed by the following function:

$$\frac{d\alpha}{dT} = \frac{1}{\beta} A \exp\left(-\frac{E}{RT}\right) f(\alpha) \quad (2)$$

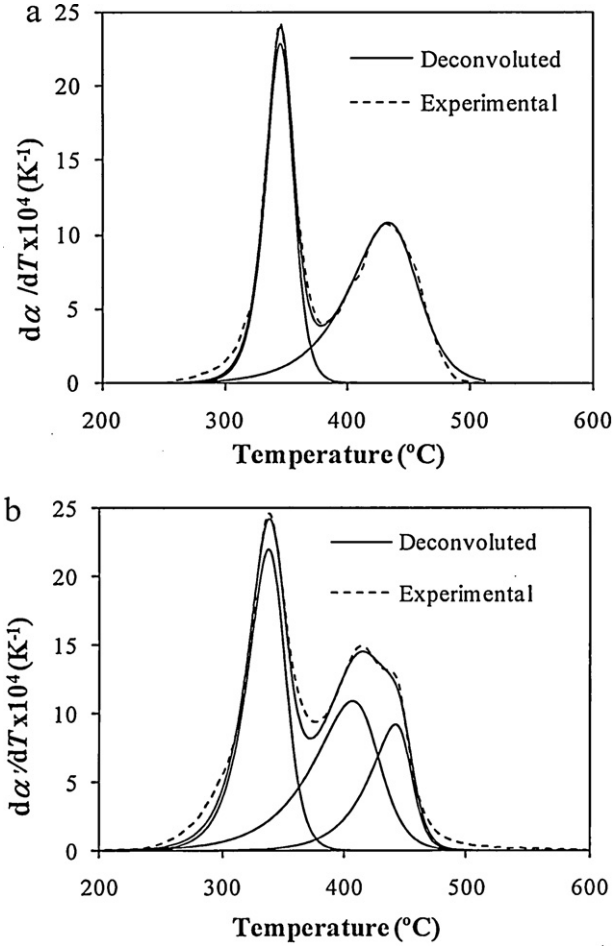

Fig. 3. Deconvolution of DTG curves corresponding to the thermal decomposition of the pristine (a) and the nanocomposite (b) samples at 5 °C/min.

where β is the heating rate, T is the absolute temperature, R the gas constant, $f(\alpha)$ the differential conversion function, and A and E the preexponential and the activation energy for the studied decomposition reaction step.

Activation energies for the three degradation steps were determined by using the Kissinger method [15], and advanced isoconversional methods such as Kissinger–Akahira–Sunose (KAS) [15,16] and Friedman [17,18], which have the advantage that don't need the knowledge of the exact thermodegradation mechanism. Integral (KAS) and differential (Friedman) isoconversional methods make use of the isoconversional principle which states that at a constant extent of conversion the reaction rate is a function only of the temperature.

The Kissinger method [15] gives the associated activation energy, E, only at the maximum of the DTG curve for each degradation step and is based on the equation:

$$\ln \frac{\beta}{T_{max}^2} = \ln \frac{AR}{E} + \ln[n(1-\alpha_{max})^{n-1}] - \frac{E}{RT_{max}} \quad (3)$$

where β is the heating rate, T_{max} is the temperature at the maximum reaction rates, α_{max} is the conversion at this T_{max} temperature, n is the reaction order and A the frequency factor. From a plot of $\ln(\beta/T_{max}^2)$ versus $1/T_{max}$ and fitting the data to a straight line, the activation energy was calculated from the slopes for each degradation step as summarized in Table 2. A good linearity was always observed with correlation coefficients of 0.9999, 0.9968 and 0.9832 for the first, second and third degradation step, respectively.

It should be pointed out that Kissinger is not an isoconversional method since the peak temperature is obtained at different heating rates, and the extent of conversion related to the peak is known to change with the heating rate [19,20]. Moreover, the determined activation energy may loss sense if it varies throughout the degradation process.

In order to calculate the activation energy during the whole process, the KAS method [15,16] was applied. This is based on the integration of Eq. (2), which after a subsequent reordering leads to the expression:

$$\ln \frac{\beta}{T^2} = \ln \left[\frac{AE}{g(\alpha)R}\right] - \frac{E}{RT} \quad (4)$$

where $g(\alpha)$ is the integral conversion function (i.e., $g(\alpha) = \int_0^\alpha (d\alpha/f(\alpha))$).

For each degree of conversion and degradation process the activation energy was obtained from the slope of the linear representation of $\ln(\beta/T^2)$ versus $1/T$. A good linearity was obtained with correlation coefficients not less than 0.97, 0.98 and 0.95 for the first, second and third degradation step, respectively. In each case the worst coefficient were found for the lowest conversion degree (0.1), whereas at a conversion of 0.95 the coefficient was in the three cases higher than 0.99. Fig. 4 plots the variation of the activation energy with the conversion for the three degradation steps. This activation energy was rather constant for the first and second degradation steps if data corresponding to the lowest conversion (lowest correlation coefficient) were not considered. It should be pointed out that at the beginning of degradation (first step and low conversion) the process may be strongly affected by the organo-modifier compound and consequently the activation energy may be lower than the average value. In the same way, low and high conversion data for the second degradation step may show some inaccuracies due to the overlapping with first and third steps, respectively. Fig. 4 shows also that the activation energy progressively increased with the conversion degree for the last degradation step. Average values of the activation energy for the three considered steps are summarized in Table 2.

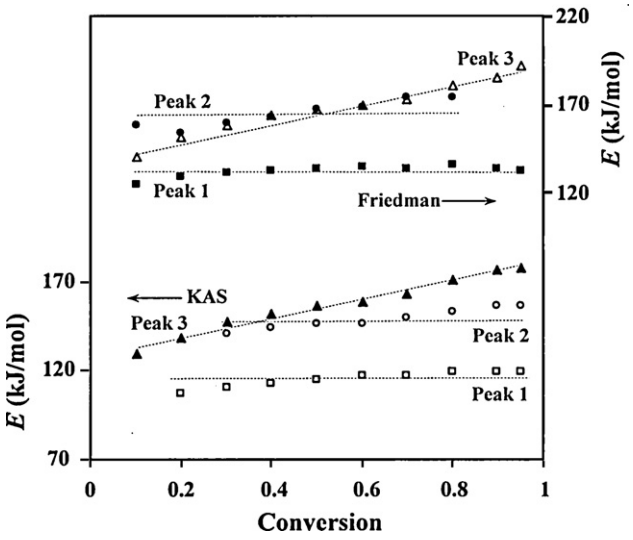

Fig. 4. Plots of the activation energy, calculated with the KAS [15,16] and Friedman [17,18] methods for the first (squares), second (circles) and third (triangles) degradation steps of the poly(glc-*alt*-amh)/C25A nanocomposite sample.

The Friedman method [17,18] (Eq. (5)) derives from the logarithmic form of the rate equation (2) and enables also to get the values of activation energies over a wide range of conversions by plotting $\ln(\beta\, d\alpha/dT)$ versus $1/T$ from thermograms recorded at several heating rates.

$$\ln \left[\beta \frac{d\alpha}{dT}\right] = \ln A + \ln f(\alpha) - \left(\frac{E}{RT}\right) \quad (5)$$

A good linearity was obtained for each conversion with correlation coefficients not less than 0.98, 0.95 and 0.98 for the first, second and third degradation step, respectively. Fig. 6 plots also the variation of the activation energy deduced from the Friedman method with the conversion for the three degradation steps. Activation energy was practically constant for the first degradation step and shows a slightly greater fluctuation for the second one, which had an overlapping with the other two steps and particularly with the third one

Table 2
Activation energies of the nanocomposite and pristine samples determined by isoconversional methods.

Sample	Step[a]	E (kJ/mol) Kissinger[b]	E (kJ/mol) KAS[c]	E (kJ/mol) Friedman[c]
Poly(glc-*alt*-amh)[d]	1	118	116	120
	2	176	179	185
Poly(glc-*alt*-amh)/C25A	1	127	111	133
	2	146	139	159
	3	168	150	168

[a] The different steps of degradation are referred to 1, 2 and 3 in increasing order of temperature.
[b] Calculated at the temperature corresponding to the maximum of each step in the DTG curve.
[c] Summarized energies correspond to mean values obtained from different degrees of conversion (from 0.1 to 0.95).
[d] From Ref. [11].

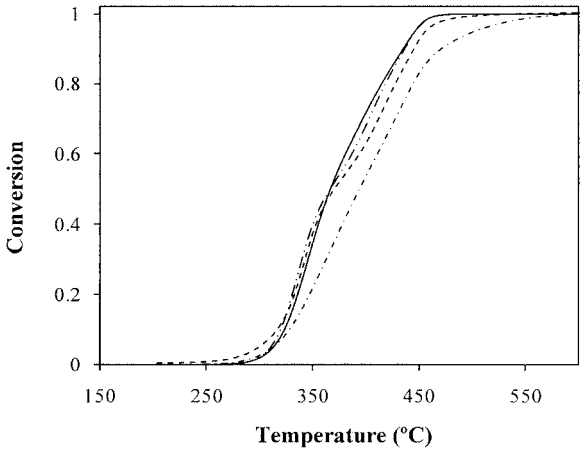

Fig. 5. Comparison between experimental (——) and simulated TG conversion curves for the poly(glc-*alt*-amh)/C25A nanocomposite sample at a representative heating rate of 5 °C/min. Curves were calculated considering the autocatalytic (– – –), $A_{3/2}$ (------) and R_2 (– – –) models for the first degradation step.

(at higher conversions). Activation energy progressively increased with the conversion degree for the last degradation step as also found in the KAS analysis. Average values of the activation energy for the three considered steps are summarized in Table 2. It can be observed that these average values were close to the single activation energy determined by the Kissinger plot, and higher than the average activation energies determined by the KAS method. Differential isoconversional methods, like Friedman, are recommended over integral when discrepancies exists [21–23]. Thus, we obtained energies of 130, 153 and 168 kJ/mol by averaging Kissinger and Friedman data for the first, second and third degradation steps, respectively.

The first degradation step had the lowest activation energy for both the neat polymer and the nanocomposite sample. The incorporation of clay particles slightly increased this activation energy. It can also be emphasized that the second stage of degradation of the neat polymer had an activation energy considerably higher than those determined in either the second or the third degradation steps of the nanocomposite sample.

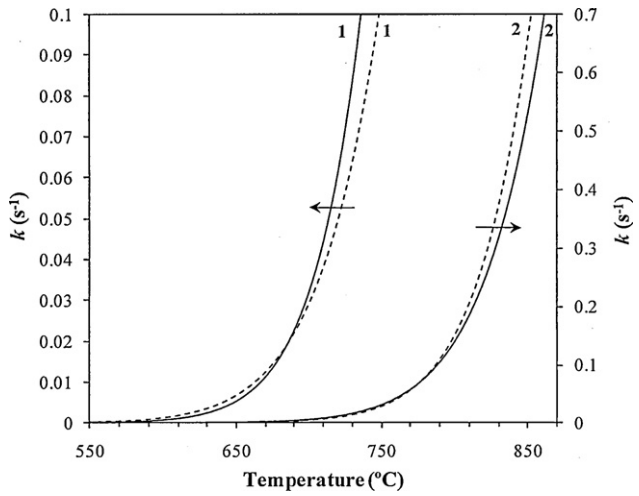

Fig. 6. Dependence of the kinetic rate constant, *k*, on temperature for the first two degradation steps (1 and 2) of the pristine (dashed lines) and the poly(glc-*alt*-amh)/C25A nanocomposite (solid lines) sample.

3.4. Thermal degradation mechanisms of the poly(glc-alt-amh)/C25A nanocomposite

The Coats–Redfern method [24] was chosen in order to determine the thermal degradation mechanism involved in the two first degradation steps of the nanocomposite. Conventional $g(\alpha)$ functions [25,26] were considered and for each one, the activation energy was calculated according to Eq. (6), which was derived considering an asymptotic approximation ($2RT/E \ll 1$).

$$\ln \frac{g(\alpha)}{T^2} = \ln\left(\frac{AR}{\beta E}\right) - \frac{E}{RT} \quad (6)$$

The Coats–Redfern equation was derived assuming that the activation energy was independent of the conversion degree, a feature that seems true for the first step of degradation and even can be considered for the second degradation step at intermediate conversion degrees.

The slope of the linear plot of $\ln g(\alpha)/T^2$ versus $1/T$ allowed the activation energy to be determined for each possible model and the model to be selected by considering the agreement with the previously calculated activation energy and the achievement of a good regression coefficient. This methodology enables to determine also the frequency factor from the intercept at the origin. The complete kinetic triplet (E, A and $f(\alpha)$) defines the variation of the degree of conversion with the temperature (Eq. (2)).

In general, calculations performed at the different heating rates showed rather similar activation energy values for each degradation step (Table 3), although a great fluctuation was found for some specific model.

Different degradation mechanisms have been deduced for the nanocomposite and the neat polymer samples, even for the common first decomposition step. Thus, the pristine polymer followed a sigmoidal A_2 mechanism [11], whereas the sigmoidal $A_{3/2}$ model, the decelerative R_2 mechanism or the autocatalytic ($n = 1.5$; $m = 0.5$) mechanism should be considered for the nanocomposite since their E values were close to those determined by the Kissinger and the Friedman method. Note that these methods gave an average activation energy of 130 kJ/mol which was within the energy range calculated for the autocatalytic model (from 100 to 130 kJ/mol), or above or below the corresponding ranges determined for the $A_{3/2}$ (from 101 to 116 kJ/mol) or the R_2 (from 136 to 142 kJ/mol) models, respectively. Discrimination between these three mechanisms should be discussed later.

The last stage of degradation of the poly(glc-*alt*-amh) sample followed an autocatalytic ($n = 1.9$; $m = 0.1$) mechanism. This decomposition process was split in other two when clay particles were added, being only possible as above indicated to analyze the mechanism for one of these two processes. Thus, a first order (F_1) mechanism could be associated to the second degradation step of the nanocomposite. It should be pointed out that, in this case, the experimental activation energy 153 kJ/mol was in agreement with only one model and consequently discrimination with other mechanisms was clear.

Table 4 summarizes the final kinetic parameters deduced for the nanocomposite at the heating rates of 2 °C/min and 40 °C/min. For the sake of completeness, previous reported data on the neat polymer are also given.

In summary, degradation of glycolic acid units (first step) took place according to an autocatalytic model, whereas a first order model described the beginning of the degradation process that involved the ω-amino acid units.

Note that clay particles should have a great influence at the beginning of degradation due to decomposition of the organomodifier and also at the end of the process (third step) due to the increasing ratio of silicate layers as the polymer decomposes. In

Table 3
Activation energies of poly(glc-*alt*-amh)/C25A obtained by the Coats–Redfern method at 2 °C/min and 40 °C/min.

	First step				Second step			
	2 °C/min		40 °C/min		2 °C/min		40 °C/min	
	E (kJ/mol)	*r*	*E* (kJ/mol)	*r*	*E* (kJ/mol)	*r*	*E* (kJ/mol)	*r*
$A_{3/2}$	101.31	0.9993	115.58	0.9988	95.43	0.9996	98.70	0.9908
A_2	73.58	0.9992	83.95	0.9987	68.82	0.9995	71.04	0.99
A_3	45.73	0.9991	52.31	0.9985	20.69	0.9878	20.69	0.9757
A_4	32.42	0.9989	36.50	0.9983	28.91	0.9994	29.55	0.9851
D_1	243.23	0.9882	232.84	0.9905	169.71	0.9949	217.63	0.9993
D_2	276.44	0.9936	281.01	0.9946	217.49	0.9982	257.14	1
D_3	294.18	0.9972	317.94	0.9973	257.21	0.9998	279.07	0.9995
D_4	275.97	0.9947	286.18	0.9954	223.36	0.9989	256.71	1
R_2	135.59	0.9952	141.85	0.9957	110.74	0.9992	125.35	0.999
R_3	142.27	0.9970	153.49	0.9971	123.08	0.9998	133.58	0.9995
F_1	156.79	0.9993	178.84	0.9989	150.73	0.9996	151.17	0.998
Power	54.06	0.9846	49.99	0.9871	41.77	0.9992	45.68	0.9991
$n = 2$	209.60	0.9959	270.45	0.9996	197.97	0.9965	210.24	0.9908
$n = 1.5$, $m = 0.5$	99.98	0.9956	129.76	0.9995	93.55	0.9962	99.17	0.9897
$n = 1.5$	181.51	0.9994	222.20	0.1000	167.36	0.9982	178.75	0.9949
$n = 1.9$, $m = 0.1$	187.68	0.9959	242.31	0.9996	177.09	0.9965	188.02	0.9906
$n = 3$	274.29	0.9834	382.59	0.9969	267.91	0.9928	281.99	0.9817

fact, the variation of the activation energy in the third step suggests a complex mechanism, which also agrees with the presence of shoulders in the corresponding DTG curve (see arrow in Fig. 2). It is well reported that clay particles had a remarkable influence on the last stages of degradation although different explanations have been postulated. In general, it is assumed that layered silicates may act as a barrier towards degradation products ablation [27,28]. Thus, the addition of clay may enhance the performance of the char formed acting as a mass transport barrier to the volatile products generated during decomposition. Alternatively, it has also been postulated that thermal stabilization is caused by a nanoconfinement effect of the clay that enhances intermolecular interactions, increases the energy barrier to molecular motion and decreases chemical reactivity [29].

The thermogravimetric trace of the C25A organo-modified clay (Fig. 2) showed that a degradation with a 30% weight loss occurred between 290 and 340 °C (DTG peak at 306 °C), an observation that demonstrates the low thermal stability of the clay. Furthermore, it is known that the thermal behaviour of nanocomposites may be affected by the stability of the organo-modifier compound used to favour the interaction between clay particles and polymer chains [30]. Decomposition products may influence the degradation mechanism of poly(glc-*alt*-amh), which on the other hand was demonstrated to be highly dependent on the copolymer composition since significant differences were previously found between the 6-aminohexanoic and the 11-aminoundecanoic derivatives [11].

3.5. Invariant activation parameters for the thermal decomposition of the poly(glc-alt-amh)/C25A nanocomposite

Kinetic parameters can also be evaluated using the IKP (invariant kinetic parameters) method [31,32]. According to this procedure, the values of the activation parameters, obtained from various forms of $f(\alpha)$, are correlated through an apparent compensation effect:

$$\ln A = \alpha^* + \beta^* E \tag{7}$$

where α^* and β^* are constants (the compensation effect parameters).

In order to apply this method, the values of $\ln A_i$ versus E_i at each heating rate (β_i) were plotted. These parameters were obtained using the Coats–Redfern methodology for the different kinetic models studied. The plot allowed the α_i^* and β_i^* constants to be determined from the intersection at the origin and the slope, respectively. Furthermore, the straight lines $\ln A_i$ versus E_i for each heating rate should intersect at a point which corresponds to the true values of A and E. These are called the invariant activation parameters (A_{inv}, E_{inv}). Certain variations of the experimental conditions actually determine a region of intersection in the $\ln A$, E space. For this reason, the evaluation of the invariant activation parameters is performed using the following relation:

$$\ln A_{inv} = \alpha^* + \beta^* E_{inv} \tag{8}$$

Table 4
Kinetic parameters associated with the different degradation steps of the poly(glc-*alt*-amh)/C25 nanocomposite and the neat polymer.

	Neat polymer[a]		Nanocomposite	
	Step 1	Step 2	Step 1	Step 2
E (kJ/mol)	111	167	100[b]–130[c]	151[b]–151[c]
$\ln A$ (min^{-1})	19.64	27.31	18.53[b]–24.41[c]	24.83[b]–25.28[c]
Model	A_2	$n = 1.9$; $m = 0.1$	$n = 1.5$; $m = 0.5$	F_1
$f(\alpha)$	$2(1-\alpha)[-\ln(1-\alpha)]^{1/2}$	$(2\alpha)^{-1}$	$\alpha^{0.5}(1-\alpha)^{1.5}$	$(1-\alpha)$
$g(\alpha)$	$[-\ln(1-\alpha)]^{1/2}$	α^2	$[(1-\alpha)/\alpha]^{-0.9}(0.5)^{-1}$	$-\ln(1-\alpha)$
E_{inv} (kJ/mol)	118	169	133	154
$\ln A_{inv}$ (min^{-1})	21.03	26.52	24.13	25.11

[a] From Ref. [11]. *E* and $\ln A$ were determined for a heating rate of 2 °C/min.
[b] Values calculated for a heating rate of 2 °C/min.
[c] Values calculated for a heating rate of 40 °C/min.

Thus, a plot of α_i^* versus β_i^* is actually a straight line whose parameters allow evaluation of the invariant activation parameters.

The IKP method can be well applied if the activation energy does not depend on the degree of conversion, which must be checked by isoconversional methods. The first degradation step of poly(glc-*alt*-amh)/C25A nanocomposite is clearly characterized by a practically constant activation energy as shown in Fig. 4 from data derived from the Friedman and indeed the KAS method, small variations being only detected at low conversion degrees. Compensation relationships for this degradation step where linear with correlation coefficient greater than 0.99 for all studied heating rates. A straight line was also observed for the α_i^* versus β_i^* plot (correlation coefficient of 0.9975) demonstrating a supercorrelation relationship for this degradation step. Furthermore, its slope indicated an E_{inv} value (Table 4) that was identical to the energy found with the isoconversional method of Friedman (133 kJ/mol).

The IKP method was also attempted for the second degradation step. Final values for the A_{inv} and E_{inv} invariant parameters are summarized in Table 4. It can be pointed out that a relative good agreement was again found between the invariant activation energy and the value deduced from the Friedman isoconversional method (i.e., 154 kJ/mol respects to 159 kJ/mol). In this way, the IKP methodology conducted to the same degradation mechanisms is deduced in the previous section.

3.6. Modeling of degradation kinetics

$d\alpha/dT$ data were calculated for each heating rate and degradation step using: the Eq. (2), the kinetic parameters (E, A and $f(\alpha)$) deduced from the Coats and Redfern method for the first and second degradation steps, and the experimental data of the third degradation step (i.e., data obtained from the deconvoluted DTG profile). The simulated DTG curve for a given heating rate was thus determined by addition of two calculated profiles (i.e., those corresponding to the first and second degradation steps), which were properly scaled to fit the experimental curve, and one experimental profile (i.e., the third degradation step). Final dependences of the degree of conversion with temperature were obtained by integration of the simulated DTG curves. Calculations were performed using the autocatalytic ($n = 1.5$; $m = 0.5$), R_2 and $A_{3/2}$ models previously postulated for the first degradation step and model F_1 for the second step, respectively. Fig. 5 compares the experimental and the simulated TG curves for a representative heating rate. Results indicated that the best agreement was obtained when the autocatalytic ($n = 1.5$; $m = 0.5$) model was considered for the first step and consequently the other two proposed mechanisms could be discarded. As shown in Fig. 5, the fitting to experimental data is good for almost the whole area, with slight divergences in the regions corresponding to the lowest and the highest weight loss.

Finally, the invariant values of the activation energies and the pre-exponential factors allowed us to calculate the rate constant, k, of the first two non-isothermal degradation steps for the nanocomposite and the neat polymer samples. Fig. 6 compares the temperature dependence of the rate constant for both studied samples and the different degradation steps.

Although for the first degradation step the nanocomposite showed higher activation energy than the neat polymer, it is clear that its pre-exponential factor was also higher (Table 4). In this way, degradation can proceed faster in the nanocomposite during the first stage of thermal decomposition. It has been claimed that an increase in the activation energy cannot be rationalized in terms of the formation of a surface silicate barrier

On the other hand, the high pre-exponential factor calculated for the second degradation step of the neat polymer justified its higher degradation rate during the last stages of decomposition despite the activation energies of both samples were quite similar and even lower for the nanocomposite (i.e., 167 kJ/mol for the neat polymer and 151 kJ/mol for the second degradation step of the nanocomposite). Note also that a similar average activation energy (168 kJ/mol) was deduced from the Friedman analysis of the third degradation step of the nanocomposite sample.

4. Conclusions

Thermal decomposition in a nitrogen atmosphere of the alternating biodegradable poly(ester amide) constituted by glycolic acid and 6-aminohexanoic acid units was significantly changed by the incorporation of a small percentage (3 wt.%) of the C25A organo-modified clay, which rendered an intercalated structure when the sample was prepared by the melt-mixing technique.

The polymer showed a first degradation step, which mainly involved the decomposition of glycolic acid units, and which proceeded faster when the clay was added. The low stability of the organo-modifier compound had a determinant role and contributed to modify the degradation mechanism associated to this step. Results derived from isoconversional analyses, and the Coats–Redfern and IKP methods were highly consistent and allowed postulating an autocatalytic mechanism when simulated degradation data were compared with the experimental curves.

Last stages of degradation proceeded slowly for the nanocomposite, which furthermore showed a complex degradation process due to the existence of two additional decomposition mechanisms. Thus, the second degradation step observed in the pristine sample was split due to the influence of clay particles which probably enhanced the performance of the char formed. The pre-exponential factor of the last degradation step of the pristine sample was higher than the calculated value for the nanocomposite suggesting that motion of reactive groups was hindered by the presence of silicate layers.

Acknowledgements

This research has been supported by grants from CICYT/FEDER and AGAUR (MAT2009-11503, 2009SGR-1208). L.M.G. acknowledges financial support from the Agència de Gestió d'Ajuts Universitaris i de Recerca.

References

[1] R.A. Gross, B. Kalra, Science 297 (2002) 803.
[2] G. F. Moore, S. M. Saunders, In Advances in Biodegradable Polymers, Rapra Review Reports 9 (1997) 2.
[3] I. Arvanitoyannis, N. Kawasaki, N. Yamamoto, Polymer 36 (1995) 857.
[4] N. Paredes, A. Rodríguez-Galán, J. Puiggalí, J. Polym. Sci. Part A: Polym. Chem. 36 (1998) 1271.
[5] R. Katsavara, V. Beridze, N. Arbuli, D. Kharadze, C.C. Chu, C.Y. Won, J. Polym. Sci. Part A: Polym. Chem. 37 (1999) 391.
[6] H.R. Stapert, A.W. Bouwens, P.J. Dijkstra, J. Feijen, Macromol. Chem. Phys. 200 (1999) 1921.
[7] M. Vera, A. Rodríguez-Galán, J. Puiggalí, Macromol. Rapid Commun. 25 (2004) 812.
[8] M. Vera, A.L. Franco, J. Puiggalí, Macromol. Chem. Phys. 205 (2004) 1782.
[9] E. Botines, M.T. Casas, J. Puiggalí, J. Polym. Sci. Part B: Polym. Phys. 45 (2007) 815.
[10] E. Botines, J. Puiggalí, Eur. Polym. J. 42 (2006) 1595.
[11] E. Botines, L. Franco, J. Puiggalí, J. Appl. Polym. Sci. 102 (2006) 5545.
[12] L. del Valle, F. Sepulcre, A. Gámez, A. Rodríguez-Galán, J. Puiggalí, Curr. Trends Polym. Sci. 12 (2008) 27.
[13] L.T. Morales, L. Franco, M.T. Casas, J. Puiggalí, J. Polym. Sci. Part A: Polym. Chem. 47 (2009) 3616.
[14] L. T. Morales, L. Franco, M. T. Casas, J. Puiggalí. Polym. Eng. Sci., in press.
[15] H.E. Kissinger, Anal. Chem. 29 (1957) 1702.
[16] T. Akahira, T. Sunose, Res. Report Chiba Inst. Technol. 16 (1971) 22.
[17] H.L. Friedman, J. Polym. Sci. Part C 6 (1964) 183.
[18] H.L. Friedman, J. Polym. Lett. 4 (1966) 323.
[19] N. Sbirrazzuoli, Y. Girault, L. Elégant, Thermochim. Acta 25 (1997) 293.
[20] S. Vyazovkin, N. Sbirrazzuoli, Macromol. Rapid Commun. 27 (2006) 1515.
[21] P. Budrugeac, D. Homentcovschi, E. Segal, J. Therm. Anal. Calorim. 63 (2000) 457.

[22] N. Sbirrazzuoli, Macromol. Chem. Phys. 208 (2007) 1592.
[23] N. Sbirrazzuoli, I. Vincent, A. Mija, N. Guido, Chemom. Intell. Lab. Syst. 96 (2009) 219.
[24] A.W. Coats, J.P. Redfern, Nature 201 (1964) 68.
[25] A.B. Phadnis, Thermochim. Acta 62 (1983) 361.
[26] S. Vyazovkin, D.J. Dollimore, Chem. Inform. Comput. Sci. 36 (1996) 42.
[27] B.N. Jang, C.A. Wilkie, Polymer 46 (2005) 2933.
[28] X. Yuan, C. Li, G. Guan, Y. Xiao, D. Zhang, Polym. Degrad. Stab. 93 (2008) 466.
[29] K. Chen, C.A. Wilkie, S. Vyazovkin, J. Phys. Chem. B 111 (2007) 12685.
[30] J.H. Chang, Y.U. An, G.S. Sur, J. Polym. Sci. Part B: Polym. Phys. 41 (2003) 94.
[31] A.I. Lesnikovich, S.V. Levchik, J. Therm. Anal. 27 (1983) 89.
[32] A.I. Lesnikovich, S.V. Levchik, J. Therm. Anal. 30 (1985) 677.